Naval Research Laboratory
Washington, DC 20375-5320

NRL/MR/6705--04-8778

Optimization and Stability Control of Relativistic and Ponderomotive Self-Channeling of Ultra-Powerful Pulses in Underdense Plasma

J. Davis

Radiation Physics and High Energy Density Materials
Plasma Physics Division

A. Borisov
C. K. Rhodes

University of Illinois, Department of Physics
Chicago, IL

August 9, 2004

REPORT DOCUMENTATION PAGE

Form Approved
OMB No. 0704-0188

1. REPORT DATE *(DD-MM-YYYY)*	2. REPORT TYPE	3. DATES COVERED *(From - To)*
9 August 2004	Memorandum report	

4. TITLE AND SUBTITLE

Optimization and Stability Control of Relativistic and Ponderomotive Self-Channeling of Ultra-Powerful Pulses in Underdense Plasma

5a. CONTRACT NUMBER

5b. GRANT NUMBER

5c. PROGRAM ELEMENT NUMBER

6. AUTHOR(S)

J. Davis, A. Borisov,* and C.K. Rhodes*

5d. PROJECT NUMBER

5e. TASK NUMBER

5f. WORK UNIT NUMBER

7. PERFORMING ORGANIZATION NAME(S) AND ADDRESS(ES)

Naval Research Laboratory, Code 6705
4555 Overlook Avenue, SW
Washington, DC 20375-5320

8. PERFORMING ORGANIZATION REPORT NUMBER

NRL/MR/6705--04-8778

9. SPONSORING / MONITORING AGENCY NAME(S) AND ADDRESS(ES)

DARPA
3701 North Fairfax Drive
Arlington, VA 22203

10. SPONSOR / MONITOR'S ACRONYM(S)

11. SPONSOR / MONITOR'S REPORT NUMBER(S)

12. DISTRIBUTION / AVAILABILITY STATEMENT

Approved for public release; distribution is unlimited.

20041008 288

13. SUPPLEMENTARY NOTES

*Laboratory for X-Ray Microimaging and Bioinformatics, Department of Physics M/C 273, University of Illinois at Chicago, Chicago, IL 60607-7059
This research was sponsored by DARPA under Job Order title: "NRLUltrabeam," MIPR 03-Q401.

14. ABSTRACT

Stable formation of multi-PW relativistic channels in underdense plasma, with the power exceeding 10^4 critical powers and the peak channel intensity in the 10^{23}W/cm^2 range, can be established using an appropriate gradient of electron density at the first stage of the self-channeling, which initiates the process of stable multi-stage relativistic and ponderomotive self-channeling.

15. SUBJECT TERMS

Laser propagation; 248 nm; Channeling; Stability

16. SECURITY CLASSIFICATION OF:			17. LIMITATION OF ABSTRACT	18. NUMBER OF PAGES	19a. NAME OF RESPONSIBLE PERSON
a. REPORT	b. ABSTRACT	c. THIS PAGE			Jack Davis
Unclassified	Unclassified	Unclassified	UL	27	19b. TELEPHONE NUMBER *(include area code)* (202) 767-3278

Standard Form 298 (Rev. 8-98)
Prescribed by ANSI Std. Z39.18

CONTENTS

OPTIMIZATION AND STABILITY CONTROL OF RELATIVISTIC AND PONDEROMOTIVE SELF-CHANNELING OF ULTRA-POWERFUL LASER PULSES IN UNDERDENSE PLASMA

Introduction

The stability analysis of relativistic and ponderomotive self-channeling of ultra-powerful laser pulses in initially uniform underdense plasmas has revealed [1-4] three major modes of the self-channeling: stable mode, with the formation of a single stable ultra-powerful channel, highly unstable mode, which is characterized by the development of multiple peripheral filaments with a power in the range of the critical power, and bifurcation mode of the self-channeling, when the transverse instability leads to the splitting of the beam into two or more powerful channels. In the case when the power of the laser beam is much greater than the critical power of the self-channeling and the radius of the beam is much bigger than the radius of the channel, the highly unstable filamentation is the dominant mode of the self-channeling. It has been established numerically and later verified experimentally, that unstable modes of the self-channeling can be converted into the stable mode using an appropriate gradient of the electron density at the initial stage of the channel formation. Our latest numerical experiments demonstrated that this technique can be used to establish optimization and stability control of multi-TW and multi-PW relativistic laser channels in underdense plasma. The stable multi-PW laser channels contain the power exceeding 10^4 critical powers and the peak relativistic channel intensity is in the 10^{23} W/cm^2 range.

The stability analysis of relativistic and ponderomotive self-channeling is based on a relatively simple model [1,5] that involves two dimensionless parameters (η, ρ_0) representing the normalized power η and normalized radius ρ_0 of the beam given by

$$\eta = P_0 / P_{cr} \qquad \text{and} \qquad \rho_0 = r_0 \omega_{p,0} / c \,. \tag{1}$$

Manuscript approved May 4, 2004.

In equation (1) P_0 and r_0 denote the peak power and the radius of the incident beam, P_{cr} represents the critical power for relativistic and ponderomotive self-channeling given by [1,5]

$$P_{cr} = (m_{e,0}^2 c^5 / e^2) \int_0^\infty g_0^2(\rho)\rho d\rho \, (\omega/\omega_{p,0})^2 = 1.6198 \times 10^{10} \, (\omega/\omega_{p,0})^2 \, W \,, \qquad (2)$$

where $m_{e,0}$, c, and e have their standard identifications, $g_0(\rho)$ is the Townes mode [6], ω is the angular frequency of the laser radiation, and $\omega_{p,0}$ represents the angular frequency of the laser radiation, given by

$$\omega_{p,0} = (4\pi e^2 N_{e,0} / m_{e,0})^{1/2} . \qquad (3)$$

The process of the self-channeling can be described as the stabilization of the transverse beam profile near one of the z-independent modes of propagation identified as the lowest eigenmodes [1,5] $U_{s,0}(\rho)$ of the governing nonlinear Schrödinger equation. The index s, $0<s<1$, is associated with normalized power η of the eigenmodes, $\rho = r\omega_{p,0}/c$ represents the normalized transverse variable, where r is the transverse coordinate. The normalized radius $\rho_{e,0}$ of the eigenmodes $U_{s,0}(\rho)$ can be defined as

$$\rho_{e,0} \equiv [2 \int_0^\infty U_{s,0}^2(\rho)\rho d\rho / U_{s,0}^2(0)]^{1/2} . \qquad (4)$$

Since eigenmodes $U_{s,0}(\rho)$ represent the normalized transverse field profile of the relativistic channels, the eigenmode curve $\rho_{e,0}(\eta)$ identifies the normalized radius of the relativistic channel as a function of normalized power trapped in the channel. Thus, the radius of the channel r_{ch} can be expressed as

$$r_{ch} = \frac{c\rho_{e,0}}{\omega_p} . \qquad (5)$$

and

$$r_{ch} = \frac{\rho_{e,0}}{2\pi}\lambda (N_e / N_{cr})^{-1/2}. \qquad (6)$$

Since $\rho_{e,0}$ varies slowly [1] for $\eta > 1.5$, we conclude that the radius of the relativistic channel scales as

$$r_{ch} \sim N_e^{-1/2}. \qquad (7)$$

From the equations (4) and (6) the peak laser intensity in the relativistic channel I_{ch} can be expressed as

$$I_{ch} = \frac{4\pi}{\rho_{e,0}^2}\frac{N_e}{N_{cr}} P_{ch}\lambda^{-2}, \qquad (8)$$

where P_{ch} represents the power trapped in the channel. Again, since $\rho_{e,0}$ varies slowly [1] for $\eta > 1.5$, the peak intensity in relativistic channels scales as

$$I_{ch} \sim \frac{N_e}{N_{cr}} P_{ch} \lambda^{-2}. \qquad (9)$$

For a constant ratio of N_e/N_{cr} we have from equations (6) and (9) the simple scaling relations

$$r_{ch} \sim \lambda, \qquad I_{ch} \sim P_{ch}\lambda^{-2}. \qquad (10)$$

The relativistic and ponderomotive self-channeling of ultra-powerful ($\eta = P_0 / P_{cr} >> 1$) laser pulses with initial radius of the beam r_0 much bigger than the radius of the channel ($r_0 >> r_{ch}$, or $\rho_0 >> \rho_{e,0}$), is typically highly unstable and results in the formation of multiple peripheral filaments. In order to establish stable channel formation and optimize the efficiency of the power compression, the good match between the incident radius of the beam and the radius of the formed channel has to be arranged:

$$r_0 \sim r_{ch} \text{ or } \rho_0 \sim \rho_{e,0}. \qquad (11)$$

The condition (11) can be achieved dynamically by the adjustment of the local electron density N_e (since $r_{ch} \sim N_e^{-1/2}$) with an appropriate longitudinal gradient in the electron density.

The major parameters of the conducted numerical stability analysis are: the incident peak power and the radius of the laser beam, the level of azimuthal perturbations in the initial transverse intensity distribution, the length of the initial stage of the self-channeling with longitudinal gradient in the electron density, the level of electron density variation and the shape of electron density profile at the initial stage, where stable ultra-powerful channels are formed. The stability analysis was performed for the perturbed Gaussian beams with incident transverse amplitude distribution given by

$$U_0(r,\phi) = I_0^{1/2} \exp(-0.5(r/r_0)^2 \times (1 + (r/r_0)^4 \sum \in_q \cos(q\phi)). \quad (12)$$

The level of weak azimuthal perturbations in equation (12) is characterized by the parameter δ_{pert} defined as

$$\delta pert = \max | I_0(r,\phi_1) - I_0(r,\phi_2) | / I_0. \quad (13)$$

For $\varepsilon_q \equiv 0.01$ (q = 1-4) in equation (12) we have $\delta_{pert} = 0.063$, and for $\varepsilon_q \equiv 0.05$ (q = 1-4) the level of azimuthal perturbations is $\delta_{pert} = 0.393$.

Results

Figure 1 illustrates the highly unstable mode of relativistic and ponderomotive self-channeling in initially uniform plasma with the formation of multiple peripheral filaments. The initial transverse intensity distribution is presented in Figure 1(a). The level of azimuthal perturbations in incident transverse intensity profile is $\delta_{pert} = 0.063$. The major laser beam and plasma parameters in this case are: $\lambda = 248$ nm, $P_0 = 39$ TW, r_0

= 10 μm, $I_0 = 1.2 \times 10^{19}$ W/cm^2, $\varepsilon_q \equiv 0.01$ (q = 1-4), $\delta_{pert} = 0.063$, $N_{e,0} = 3.8 \times 10^{20}$ cm^{-3}. The normalized power and beam radius in this case are $\eta = P_0 / P_{cr} \cong 50$, $\rho_0 \cong 20$. Figure 1(b) depicts the transverse profile with multiple peripheral relativistic filaments evolved in the process of highly unstable relativistic and ponderomotive self-channeling. The stability of the self-channeling and efficient power compression can be established by introduction of multi-stage self-channeling. The first stage, which initiates the stable channel formation, involves the exponential longitudinal gradient in electron density profile defined by $N_{e,0}(z) = N_{e,0}(0)\exp(\alpha z)$ with $N_{e,o}(0) = 1.9 \times 10^{19}$ cm^{-3}, $N_{e,0,max} = 3.8 \times 10^{20}$ cm^{-3}. All parameters of the laser beam are the same as in the previous case presented in Figure 1. The dynamics of stable self-channeling of the laser beam from Figure 1(a) in the plasma with longitudinal electron density profile is presented in Figure 2. It is evident that highly unstable structure with multiple filaments (see Figure 1(b)) has been transformed into the formation of stable ultra-powerful laser channel. Our numerical modeling demonstrated that similar stable channel formation can be established in the multi-PW range. Figure 3 illustrates the formation of stable multi-PW relativistic laser channel at the initial stage of relativistic and ponderomotive self-channeling involving longitudinal gradient in the electron density. The major laser beam and plasma parameters in this case are: λ = 248 nm, $P_0 = 7.8$ PW, $r_0 = 2$ μm, $I_0 = 6.2 \times 10^{22}$ W/cm^2, $\varepsilon_q \equiv 0.01$ (q = 1-4), $\delta_{pert} = 0.063$, $N_{e,0}(0) = 5.0 \times 10^{19}$ cm^{-3}, $N_{e,0,max} = 3.8 \times 10^{20}$ cm^{-3}. The initial power of the laser pulse P_0 is $P_0 = 10^4 P_{cr}$, and the power trapped in the stable relativistic channel P_{ch} is in the same range. In this case, the longitudinal profile of the electron density at the initial stage of the relativistic and ponderomotive self-channeling has an exponential shape defined by $N_{e,0}(z) = N_{e,0}(0) \times \exp(\alpha z)$. The performed

numerical experiments demonstrated, that for laser pulse and plasma parameters corresponding to Figure 3, stability of the multi-PW relativistic channel formation can be established with the various shapes of the electron density profile at the initial stage of the self-channeling. One of the results is presented in Figure 4, which demonstrates the process of stable relativistic and ponderomotive self-channeling with electron density profile defined by

$$N_{e,0}(z) = N_{e,0}(0)\{ N_{e,0,max}/N_{e,0}(0) - (N_{e,0,max}/N_{e,0}(0) - 1)\times\exp[-(z/z_{exp,2})^2]\}, \quad (14)$$

with $N_{e,0,max}/N_{e,0}(0) = 7.6$ and $z_{exp,2} = 300$ μm. All major laser pulse and plasma parameters are the same as in the case presented in Figure 3. Stable multi-PW relativistic laser channel presented in Figure 4 contains power in the order of 10^4 critical powers.

The process of stable formation of multi-PW relativistic channels with the power exceeding 10^4 P_{cr} is presented in Figure 5. The major laser beam and plasma parameters in this case are: $\lambda = 248$ nm, $P_0 = 9$ PW, $r_0 = 5$ μm, $I_0 = 1.1 \times 10^{22}$ W/cm^2, $\varepsilon_q \equiv 0.01$ (q = 1-4), $\delta_{pert} = 0.063$, $N_{e,0}(0) = 7.6 \times 10^{18}$ cm^{-3}, $N_{e,0,max} = 3.8 \times 10^{20}$ cm^{-3}. The longitudinal profile of the electron density at the initial stage of the relativistic and ponderomotive self-channeling has an exponential shape defined by $N_{e,0}(z) = N_{e,0}(0) \times \exp(\alpha z)$. The transverse profile of the incident laser beam and transverse profile of evolved stable multi-PW relativistic laser channel are presented in Figure 5(a) and Figure 5(b), respectively. Figure 5(c) illustrates the process of stable channel formation. The trajectory of stable relativistic and ponderomotive self-channeling in the plane of dimensionless parameters (η, ρ_0) (see equation (1)) is presented in Figure 5(d). It is evident from the position of point B_{Stable} that the stable multi-PW relativistic channel

depicted in Figure 5(b) contains more than 10^4 critical powers. Note, that the peak intensity in the channel exceeds 10^{23} W/cm^2.

Our numerical experiments demonstrated that the same approach, involving initial stage of the self-channeling with longitudinal electron density profile, results in stable multi-PW relativistic channel formation even in the case of severely distorted incident laser beams with relatively big initial beam radius. Figure 6 illustrates one of these examples. The major laser beam and plasma parameters in this case are: $\lambda = 248$ nm, $P_0 = 9$ PW, $r_0 = 5$ μm, $I_0 = 1.0 \times 10^{22}$ W/cm^2, $\varepsilon_q \equiv 0.05$ (q = 1-4), $\delta_{pert} = 0.393$, $N_{e,0}(0) = 9.5 \times 10^{17}$ cm^{-3}, $N_{e,0,max} = 3.8 \times 10^{20}$ cm^{-3}. The longitudinal profile of the electron density at the initial stage of the relativistic and ponderomotive self-channeling has an exponential shape defined by $N_{e,0}(z) = N_{e,0}(0) \times \exp(\alpha z)$. The strongly azimuthally perturbed transverse intensity profile of the incident laser beam is presented in Figure 6(a). The transverse profile of the evolved stable multi-PW relativistic channel is depicted in Figure 6(b). Figure 6(c) demonstrates the dynamics of stable channel formation in the case of severely azimuthally aberrated incident multi-PW laser beams with relatively big initial beam radius.

Summary

In conclusion, detailed studies of the transverse stability of relativistic and ponderomotive self-channeling have demonstrated that multi-stage self-channeling, with the initial stage involving an appropriate gradient in the electron density profile, results in stable formation of multi-PW relativistic channels in underdense plasma with power exceeding 10^4 critical powers and peak channel intensity in the 10^{23} W/cm^2 range.

Acknowledgement

The authors thank Dr. Martin Stickley for his support and encouragement. This work was supported by DARPA.

REFERENCES

1. A. B. Borisov, O.B. Shiryaev, A. McPherson, K. Boyer, and C. K. Rhodes, "Stability Analysis of Relativistic and Charge-Displacement Self-Channeling of Intense Laser Pulses In Underdense Plasmas," *Plasma Phys. Control. Fusion* **37,** 56 (1995).
2. A. B. Borisov, J. W. Longworth, K. Boyer, and C. K. Rhodes, "Stable Relativistic/Charge-Displacement Channels In Ultrahigh Power Density (~10^{21} W/cm ^{3}) Plasmas," *Proc. Acad. Sci. USA* **95,** 7854 (1998).
3. A. B. Borisov, S. Cameron, Y. Dai, J. Davis, T. Nelson, W. A. Schroeder, J. W. Longworth, K. Boyer, and C. K. Rhodes, "Dynamics of Optimized Stable Channel Formation of Intense Laser Pulses with the Relativistic/Charge-Displacement Mechanism," *J. Phys. B: At. Mol. Opt. Phys.* **32,** 3511 (1999).
4. A. B. Borisov, S. Cameron, T. S. Luk, T. R. Nelson, A. J. Van Tassle, J. Santoro, W. A. Schroeder, Y. Dai, J. W. Longworth, K. Boyer, and C. K. Rhodes, "Bifurcation Mode of Relativistic and Charge-Displacement Self-Channeling," *J. Phys. B: At. Mol. Opt. Phys.* **34,** 2167 (2001).
5. A. B. Borisov, A. V. Borovskiy, O. B. Shiryaev, V. V. Korobkin, A. M. Prokhorov, J. C. Solem, T. S. Luk, K. Boyer, and C. K. Rhodes, "Relativistic and Charge-Displacement Self-Channeling of Intense Ultrashort Laser Pulses in Plasmas," *Phys. Rev. A* **45**, 5830 (1992).
6. R. Y. Chiao, E. Garmire, and C. H. Townes, "Self-Trapping of Optical Beams," *Phys. Rev. Lett.* **13**, 479 (1964).

CAPTIONS

Figure 1. Highly unstable relativistic and ponderomotive self-channeling of azimuthally perturbed multi-TW laser pulse in initially uniform underdense plasma. The laser and plasma parameters are: $\lambda = 248$ nm, $P_0 \cong 39$ TW, $r_0 = 10$ μm, $I_0 = 1.2 \times 10^{19}$ W/cm^2, $N_{e,0} = 3.8 \times 10^{20}$ cm^{-3}. The normalized power and beam radius in this case are $\eta = P_0 / P_{cr} \cong 50$, $\rho_0 \cong 20$. The incident azimuthally perturbed transverse amplitude distribution is defined by the equation (12) with $\varepsilon_q \equiv 0.01$ (q = 1-4). The corresponding level of weak azimuthal perturbations is characterized by δ_{pert} from the equation (13), $\delta_{pert} = 0.063$. Panel (a) shows weekly azimuthally perturbed transverse intensity profile of the incident laser beam. Panel (b) demonstrates the transverse structure with multiple peripheral filaments evolved in the process of highly unstable relativistic and ponderomotive self-channeling.

Figure 2. Dynamics of stable multi-TW relativistic channel formation at the initial stage of the self-channeling with exponential longitudinal electron density profile defined by $N_{e,0}(z) = N_{e,0}(0)\exp(\alpha z)$ with $N_{e,o}(0) = 1.9 \times 10^{19}$ cm^{-3}, $N_{e,0,max} = 3.8 \times 10^{20}$ cm^{-3}. All laser pulse parameters are the same as in the previous case depicted in Figure 1: $\lambda = 248$ nm, $P_0 = 39$ TW, $r_0 = 10$ μm, $I_0 = 1.2 \times 10^{19}$ W/cm^2. The incident azimuthally perturbed transverse intensity profile is the same as the distribution from Figure 1(a) with $\varepsilon_q \equiv 0.01$ (q = 1-4) and $\delta_{pert} = 0.063$ (see equations (12) and (13)). The dynamics of stable relativistic channel formation is presented in (x,z) plane, where z is the axis of propagation and x is one of the transverse coordinates.

Figure 3. Dynamics of stable multi-PW relativistic channel formation at the initial stage of the self-channeling with exponential longitudinal electron density profile defined by $N_{e,0}(z) = N_{e,0}(0)\exp(\alpha z)$ with $N_{e,o}(0) = 5 \times 10^{19}$ cm^{-3}, $N_{e,0,max} = 3.8 \times 10^{20}$ cm^{-3}. Laser pulse parameters are: $\lambda = 248$ nm, $P_0 = 7.8$ PW, $r_0 = 2$ μm, $I_0 = 6.2 \times 10^{22}$ W/cm^2. The incident azimuthally perturbed transverse amplitude distribution is defined by the equation (12) with $\varepsilon_q \equiv 0.01$ (q = 1-4). The corresponding level of azimuthal perturbations is $\delta_{pert} = 0.063$ (see equation (13)). The power trapped in the stable relativistic multi-PW laser channel is in the range of 10^4 critical powers.

Figure 4. Dynamics of stable multi-PW relativistic channel formation at the initial stage of the self-channeling with longitudinal electron density profile defined by the equation (14) with $N_{e,o}(0) = 5 \times 10^{19}$ cm^{-3}, $N_{e,0,max} = 3.8 \times 10^{20}$ cm^{-3}, and $z_{exp,2} = 300$ μm. Laser pulse parameters are the same as in the previous case illustrated in Figure 3: $\lambda = 248$ nm, $P_0 = 7.8$ PW, $r_0 = 2$ μm, $I_0 = 6.2 \times 10^{22}$ W/cm^2. The incident azimuthally perturbed transverse amplitude distribution is defined by the equation (12) with $\varepsilon_q \equiv 0.01$ (q = 1-4). The corresponding level of azimuthal perturbations is $\delta_{pert} = 0.063$ (see equation (13)). The power trapped in the stable relativistic multi-PW laser channel is in the range of 10^4 critical powers.

Figure 5. Stable multi-PW relativistic channel formation at the initial stage of the self-channeling with exponential longitudinal electron density profile defined by $N_{e,0}(z) = N_{e,0}(0)\exp(\alpha z)$ with $N_{e,o}(0) = 1.9 \times 10^{19}$ cm^{-3}, $N_{e,0,max} = 3.8 \times 10^{20}$ cm^{-3}. Laser pulse

parameters are: $\lambda = 248$ nm, $P_0 = 9$ PW, $r_0 = 5$ μm, $I_0 = 1.1 \times 10^{22}$ W/cm^2. The incident azimuthally perturbed transverse amplitude distribution is defined by the equation (12) with $\varepsilon_q \equiv 0.01$ (q = 1-4). The corresponding level of azimuthal perturbations is $\delta_{pert} = 0.063$ (see equation (13)). Panel (a) shows the incident azimuthally perturbed transverse intensity profile. The transverse profile of the evolved stable multi-PW relativistic channel is presented in Panel (b). Panel (c) demonstrates the dynamics of stable channel formation in (x,z) plane, where z is the axis of propagation and x is one of the transverse coordinates. The trajectory of stable relativistic and ponderomotive self-channeling in the (η, ρ_0) plane (see equation (1)) is depicted in Panel (d). The power of the evolved stable multi-PW relativistic channel exceeds 10^4 critical powers. The peak channel intensity is in the 10^{23} W/cm^2 range.

Figure 6. Stable relativistic channel formation in the case of severely azimuthally aberrated incident multi-PW laser beam with relatively big initial beam radius. The exponential longitudinal electron density profile is defined by $N_{e,0}(z) = N_{e,0}(0)\exp(\alpha z)$ with $N_{e,o}(0) = 9.5 \times 10^{17}$ cm^{-3}, $N_{e,0,max} = 3.8 \times 10^{20}$ cm^{-3}. Laser pulse parameters are: $\lambda = 248$ nm, $P_0 = 9$ PW, $r_0 = 5$ μm, $I_0 = 1.0 \times 10^{22}$ W/cm^2. The incident severely distorted transverse amplitude distribution is defined by the equation (12) with $\varepsilon_q \equiv 0.05$ (q = 1-4). The corresponding level of azimuthal perturbations is $\delta_{pert} = 0.393$ (see equation (13)). The strongly azimuthally perturbed transverse intensity profile of the incident laser beam is presented in Panel (a). The transverse profile of the evolved stable multi-PW relativistic channel is presented in Panel (b). Panel (c) demonstrates in (x,z) plane the dynamics of stable relativistic and ponderomotive self-channeling of severely

azimuthally aberrated incident multi-PW laser beam with relatively big initial beam radius. The power of the evolved stable multi-PW relativistic channel exceeds 10^4 critical powers. The peak channel intensity is in the 10^{23} W/cm^2 range.

$\lambda = 248$ nm, $P_0 = 39$ TW, $r_0 = 10.0$ μm, $P_0 / P_{cr} \cong 50$
$I_0 = 1.2 \times 10^{19}$ W/cm^2, $\delta_{perturbations} = 0.063$
$N_{e,0} = 3.8 \times 10^{20}$ cm^{-3}
Initially Uniform Electron Density

Initial Transverse Intensity Profile

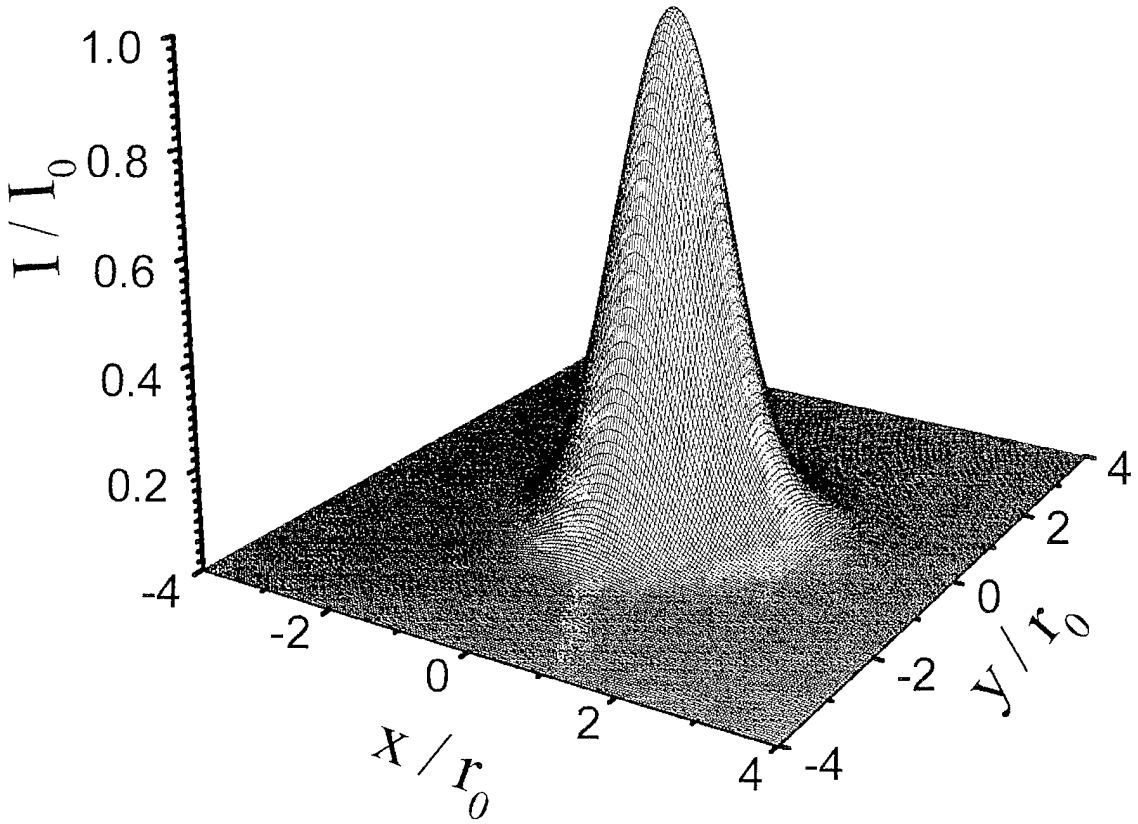

Figure 1(a)

$\lambda = 248$ nm, $P_0 = 39$ TW, $r_0 = 10.0$ μm, $P_0 / P_{cr} \cong 50$
$I_0 = 1.2 \times 10^{19}$ W/cm^2, $\delta_{perturbations} = 0.063$
$N_{e,0} = 3.8 \times 10^{20}$ cm^{-3}
Initially Uniform Electron Density

Transverse Profile of Multiple Relativistic Filaments

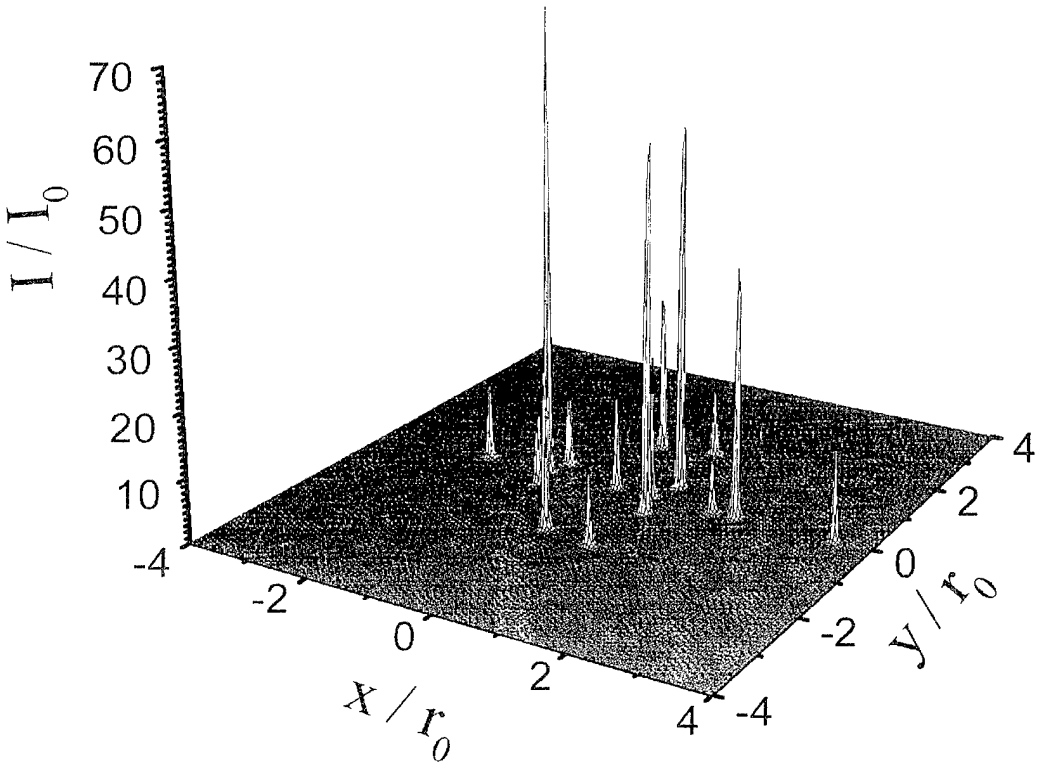

Figure 1(b)

$\lambda = 248$ nm, $P_0 = 39$ TW, $r_0 = 10.0$ μm
$I_0 = 1.2 \times 10^{19}$ W/cm^2, $\delta_{perturbations} = 0.063$
$N_{e,0}(0) = 1.9 \times 10^{19}$ cm^{-3}, $N_{e,0,max} = 3.8 \times 10^{20}$ cm^{-3}

Longitudinal Gradient in Electron Density
$N_{e,0}(z) = N_{e,0}(0) \times \exp(\alpha z)$
$N_{e,0,max} / N_{e,0}(0) = 20$, $z_{max} = 2000$ μm

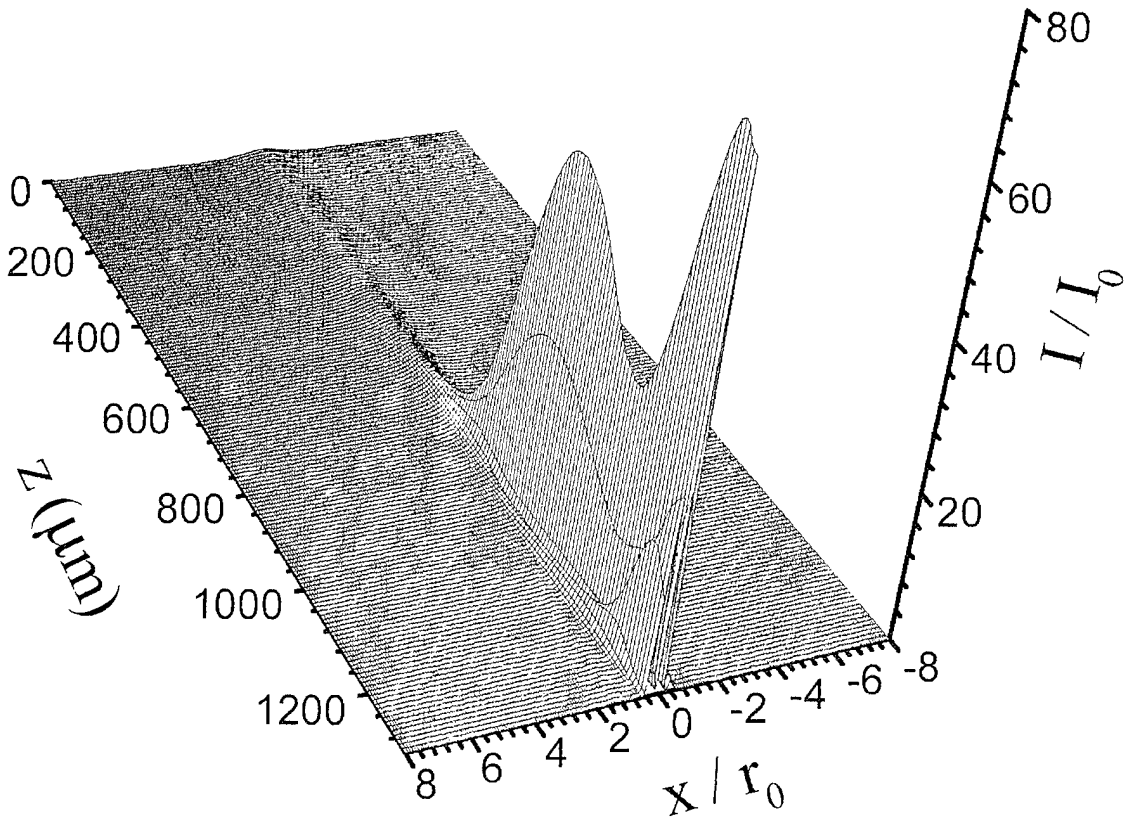

Figure 2

$\lambda = 248$ nm
$P_0 = 7.8$ PW
$r_0 = 2.0$ μm
$I_0 = 6.2 \times 10^{22}$ W/cm^2
$N_{e,0}(0) = 5 \times 10^{19}$ cm^{-3}
$N_{e,0,max} = 3.8 \times 10^{20}$ cm^{-3}
Longitudinal Gradient in Electron Density

$P_{Channel} / P_{cr} \sim 10000$

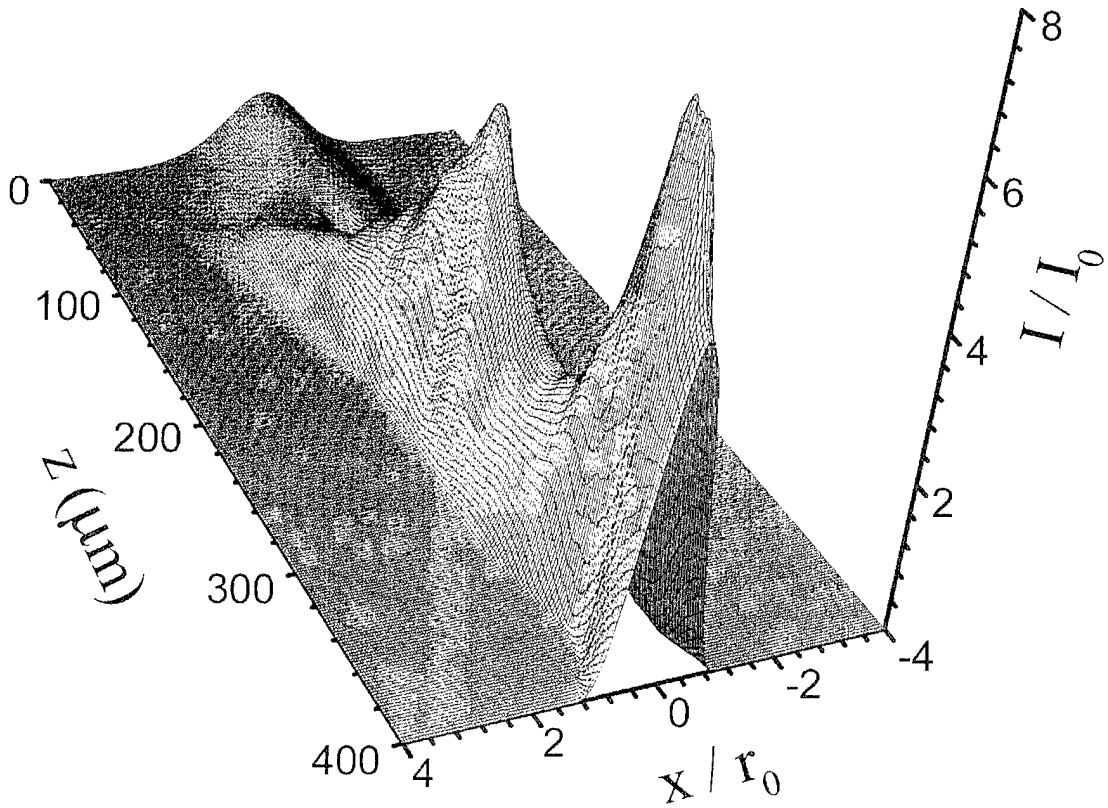

Figure 3

$\lambda = 248$ nm
$P_0 = 7.8$ PW
$r_0 = 2.0$ μm
$I_0 = 6.2 \times 10^{22}$ W/cm^2
$N_{e,0}(0) = 5 \times 10^{19}$ cm^{-3}
$N_{e,0,max} = 3.8 \times 10^{20}$ cm^{-3}
Longitudinal Gradient in Electron Density

$$P_{Channel} / P_{cr} \sim 10000$$

$N_{e,0}(z) = N_{e,0,max} [1-(1-N_{e,0}(0)/N_{e,0,max})*\exp(-(z/z_{exp,2})^2)]$
$N_{e,0}(0)/N_{e,0,max} = 1/7.6$, $z_{exp,2} = 300$ μm

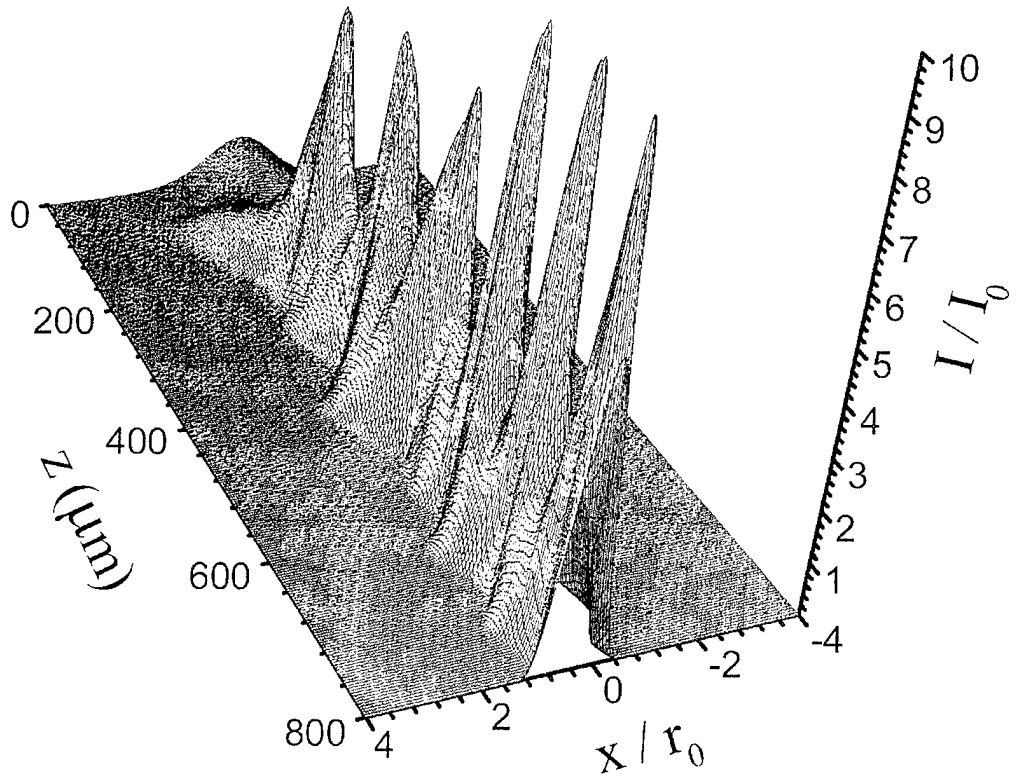

Figure 4

$\lambda = 248$ nm, $P_0 = 9.0$ PW, $r_0 = 5.0$ μm
$I_0 = 1.1 \times 10^{22}$ W/cm^2, $\delta_{perturbations} = 0.0629$
$N_{e,0}(0) = 7.6 \times 10^{18}$ cm^{-3}, $N_{e,0,max} = 3.8 \times 10^{20}$ cm^{-3}

Longitudinal Gradient in Electron Density
$N_{e,0}(z) = N_{e,0}(0) \times \exp(\alpha z)$
$N_{e,0,max} / N_{e,0}(0) = 50$, $z_{max} = 1500$ μm

Initial Transverse Intensity Profile

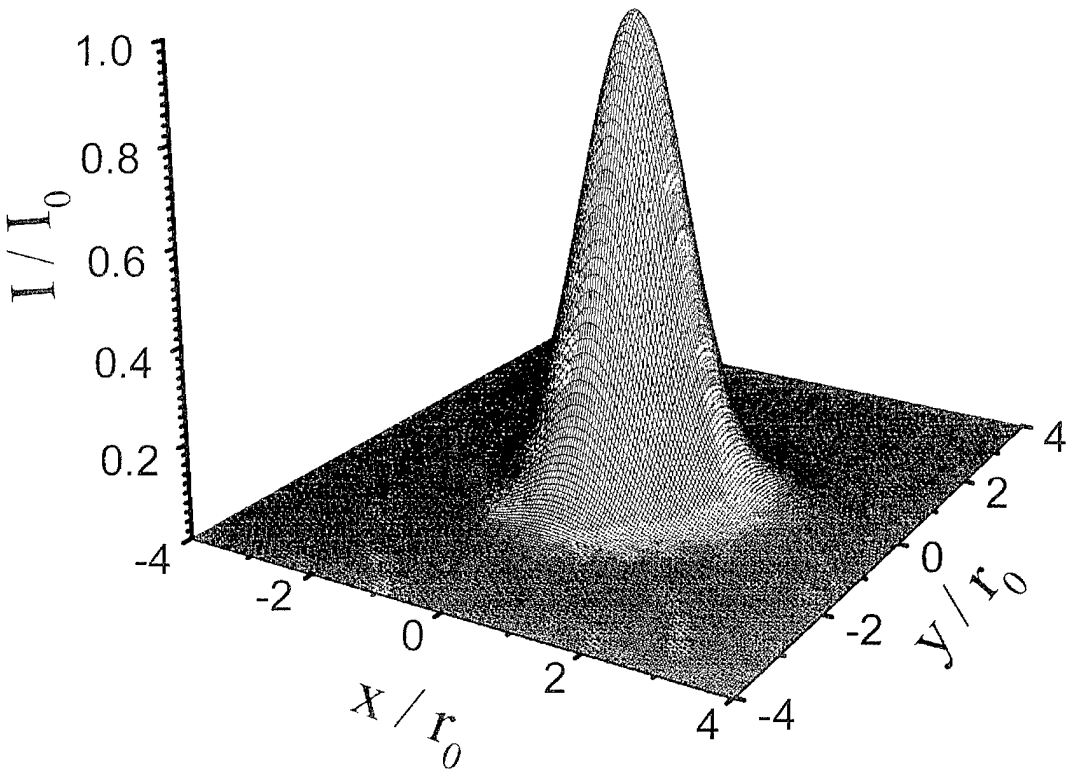

Figure 5(a)

$\lambda = 248$ nm, $P_0 = 9.0$ PW, $r_0 = 5.0$ μm
$I_0 = 1.1 \times 10^{22}$ W/cm^2, $\delta_{perturbations} = 0.0629$
$N_{e,0}(0) = 7.6 \times 10^{18}$ cm^{-3}, $N_{e,0,max} = 3.8 \times 10^{20}$ cm^{-3}

Longitudinal Gradient in Electron Density
$N_{e,0}(z) = N_{e,0}(0) \times \exp(\alpha z)$
$N_{e,0,max} / N_{e,0}(0) = 50$, $z_{max} = 1500$ μm

Stable Relativistic Channel Profile
$P_{Channel} / P_{Critical} \gtrsim 10000$

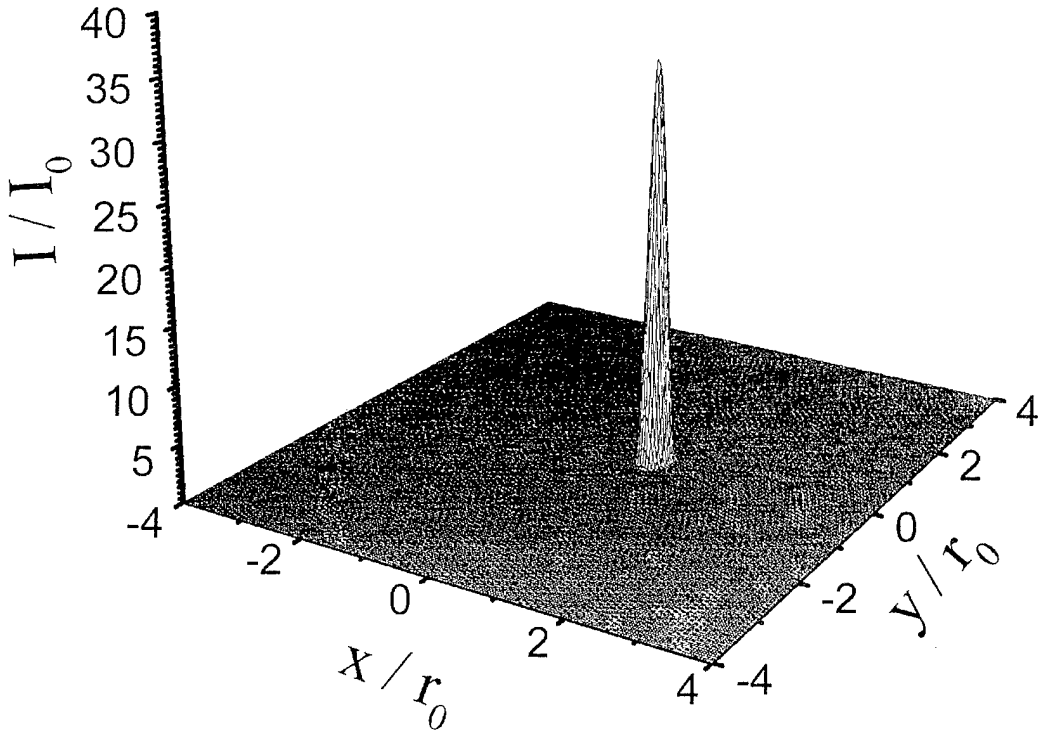

Figure 5(b)

$\lambda = 248$ nm, $P_0 = 9.0$ PW, $r_0 = 5.0$ μm
$I_0 = 1.1 \times 10^{22}$ W/cm^2, $\delta_{perturbations} = 0.063$
$N_{e,0}(0) = 7.6 \times 10^{18}$ cm^{-3}, $N_{e,0,max} = 3.8 \times 10^{20}$ cm^{-3}

Longitudinal Gradient in Electron Density
$N_{e,0}(z) = N_{e,0}(0) \times \exp(\alpha z)$
$N_{e,0,max} / N_{e,0}(0) = 50$, $z_{max} = 1500$ μm

$P_{critical} / P_{initial} \geq 1000$

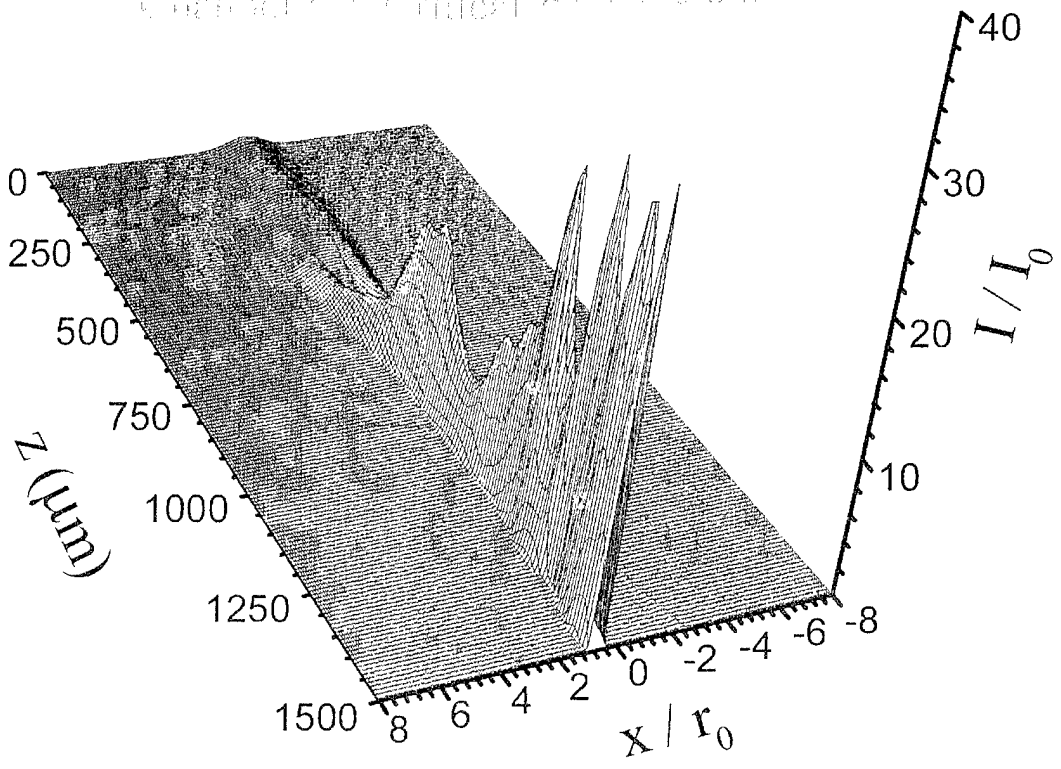

Figure 5©

$\lambda = 248$ nm, $P_0 = 9.0$ PW, $r_0 = 5.0$ μm
$I_0 = 1.1 \times 10^{22}$ W/cm^2, $\delta_{perturbations} = 0.063$
$N_{e,0}(0) = 7.6 \times 10^{18}$ cm^{-3}, $N_{e,0,max} = 3.8 \times 10^{20}$ cm^{-3}

Longitudinal Gradient in Electron Density
$N_{e,0}(z) = N_{e,0}(0) \times \exp(\alpha z)$
$N_{e,0,max} / N_{e,0}(0) = 50$, $z_{max} = 1500$ μm

$P_{Channel} / P_{Critical} \gtrsim 10000$

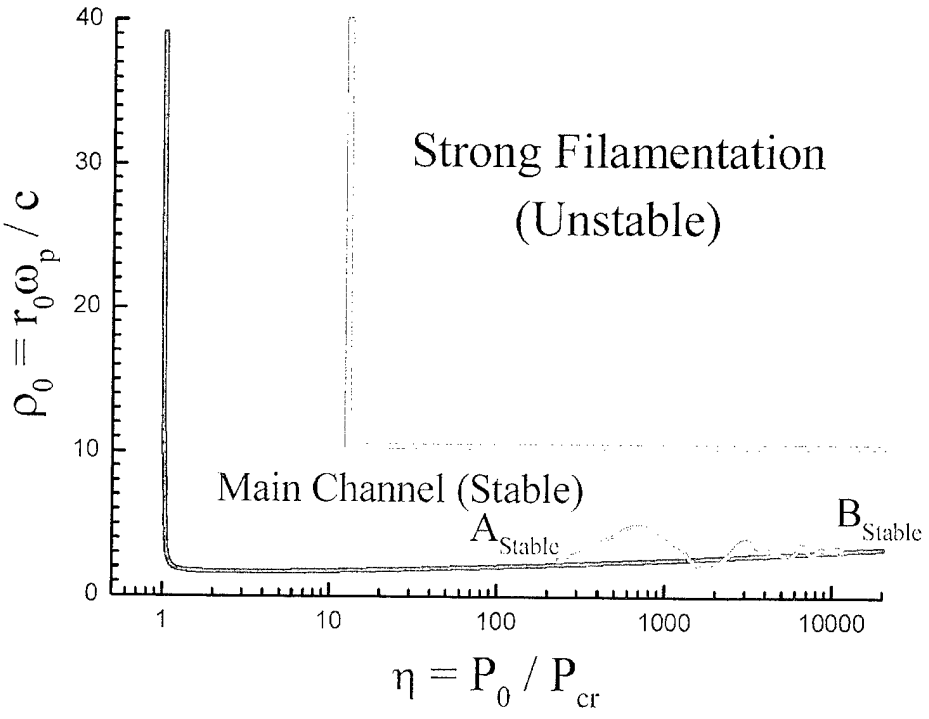

Figure 5(d)

$\lambda = 248$ nm, $P_0 = 9.0$ PW, $r_0 = 5.0$ μm
$I_0 = 1.0 \times 10^{22}$ W/cm^2, $\delta_{perturbations} = 0.393$
$N_{e,0}(0) = 9.5 \times 10^{17}$ cm^{-3}, $N_{e,0,max} = 3.8 \times 10^{20}$ cm^{-3}

Longitudinal Gradient in Electron Density
$N_{e,0}(z) = N_{e,0}(0) \times \exp(\alpha z)$
$N_{e,0,max} / N_{e,0}(0) = 400$, $z_{max} = 5000$ μm

Initial Transverse Intensity Profile

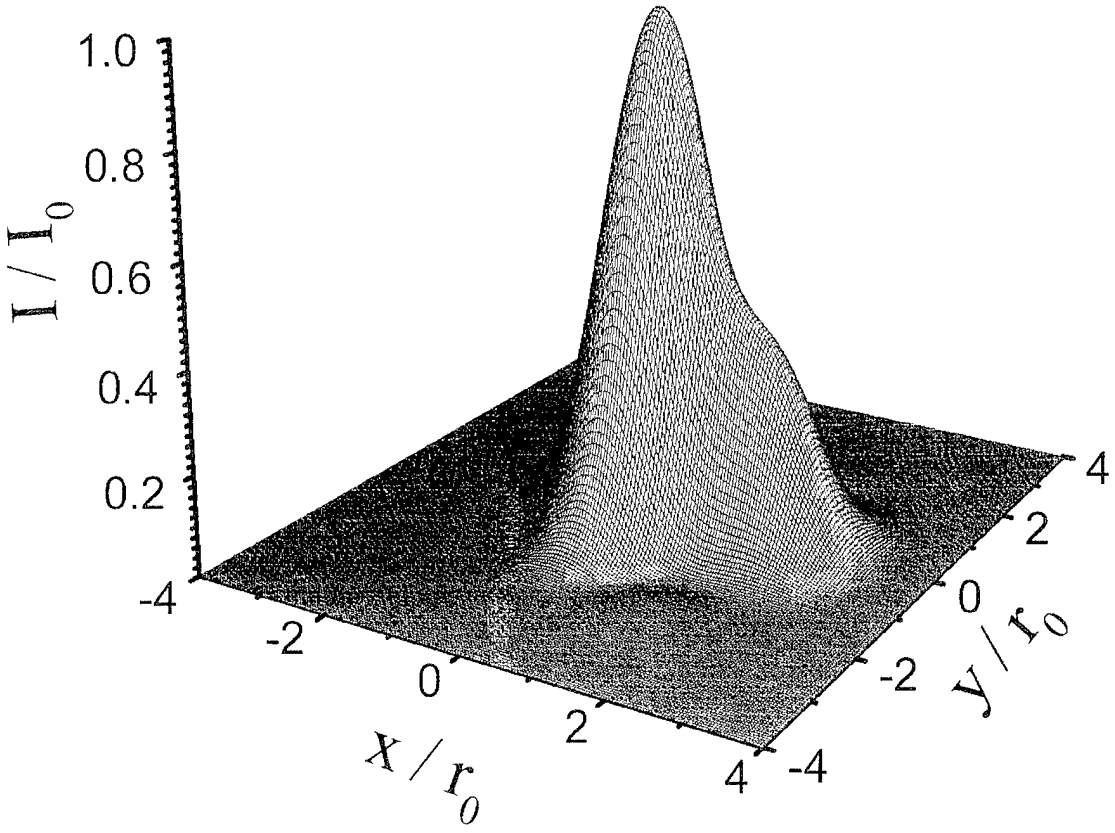

Figure 6(a)

$\lambda = 248$ nm, $P_0 = 9.0$ PW, $r_0 = 5.0$ μm
$I_0 = 1.0 \times 10^{22}$ W/cm^2, $\delta_{perturbations} = 0.393$
$N_{e,0}(0) = 9.5 \times 10^{17}$ cm^{-3}, $N_{e,0,max} = 3.8 \times 10^{20}$ cm^{-3}

Longitudinal Gradient in Electron Density
$N_{e,0}(z) = N_{e,0}(0) \times \exp(\alpha z)$
$N_{e,0,max} / N_{e,0}(0) = 400$, $z_{max} = 5000$ μm

Stable Relativistic Channel Profile
$P_{Channel} / P_{Critical} \sim 10000$

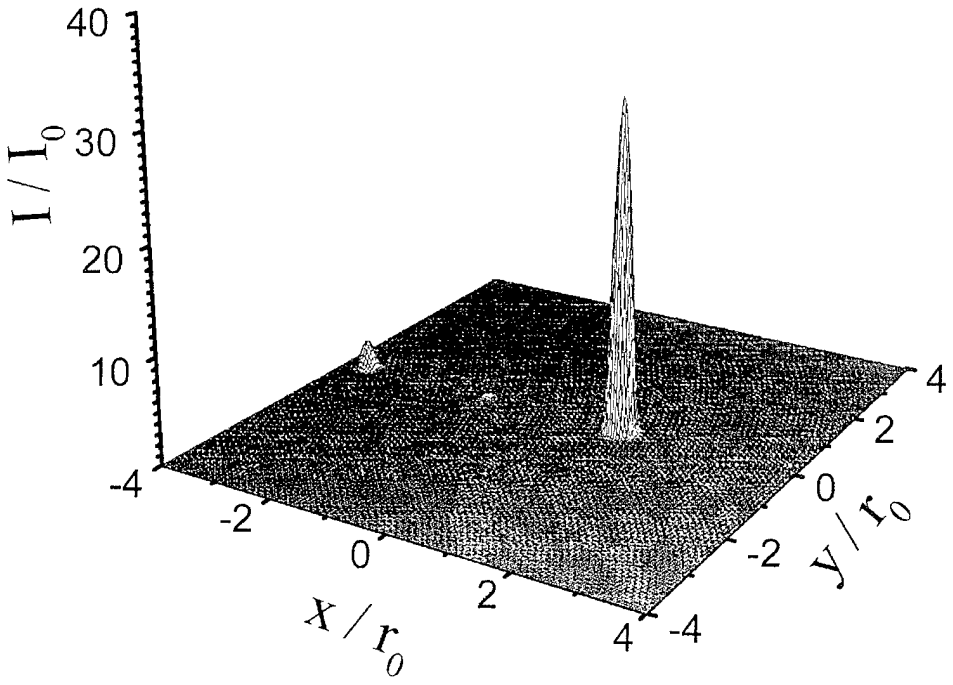

Figure 6(b)

$\lambda = 248$ nm, $P_0 = 9.0$ PW, $r_0 = 5.0$ μm
$I_0 = 1.0 \times 10^{22}$ W/cm^2, $\delta_{perturbations} = 0.393$
$N_{e,0}(0) = 9.5 \times 10^{17}$ cm^{-3}, $N_{e,0,max} = 3.8 \times 10^{20}$ cm^{-3}

Longitudinal Gradient in Electron Density
$N_{e,0}(z) = N_{e,0}(0) \times \exp(\alpha z)$
$N_{e,0,max} / N_{e,0}(0) = 400$, $z_{max} = 5000$ μm

$P_{channel} / P_{critical} = 10.70$

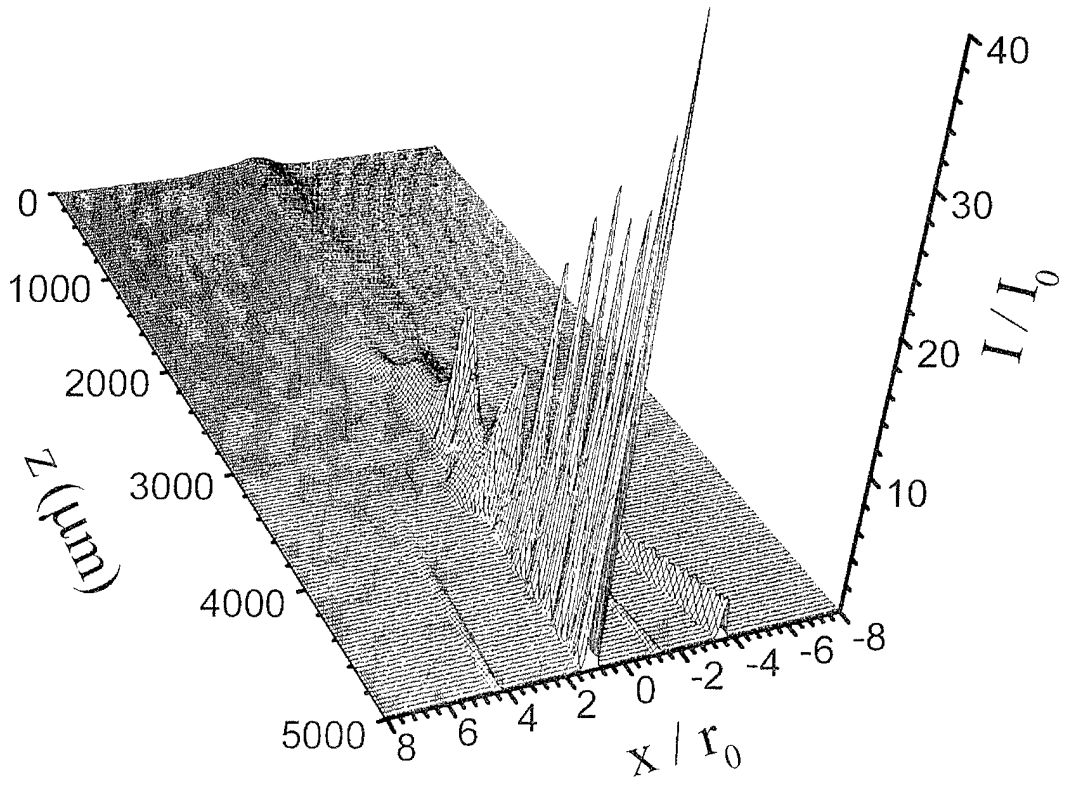

Figure 6(c)